JGR Biogeosciences

RESEARCH ARTICLE
10.1029/2022JG007352

Accounting for Changes in Radiation Improves the Ability of SIF to Track Water Stress-Induced Losses in Summer GPP in a Temperate Deciduous Forest

Zachary Butterfield[1], Troy Magney[2], Katja Grossmann[3], Gil Bohrer[4], Chris Vogel[5], Stephen Barr[1], and Gretchen Keppel-Aleks[1]

[1]Climate and Space Sciences and Engineering, University of Michigan, Ann Arbor, MI, USA, [2]Department of Plant Sciences, University of California, Davis, Davis, CA, USA, [3]Institute of Environmental Physics, University of Heidelberg, Heidelberg, Germany, [4]Civil, Environmental and Geodetic Engineering, Ohio State University, Columbus, OH, USA, [5]University of Michigan Biological Station, Pellston, MI, USA

Abstract Global observations of solar-induced chlorophyll fluorescence (SIF) are available from multiple satellite platforms, and SIF is increasingly used as a proxy for photosynthetic activity and ecosystem productivity. Because the relationship between SIF and gross primary productivity (GPP) depends on a variety of factors including ecosystem type and environmental conditions, it is necessary to study SIF observations across various spatiotemporal scales and ecosystems. To explore how SIF signals relate to productivity over a temperate deciduous forest, we deployed a PhotoSpec spectrometer system at the University of Michigan Biological Station AmeriFlux site (US-UMB) in the northern Lower Peninsula of Michigan during the 2018 and 2019 growing seasons. We found that SIF correlated with GPP across diurnal and seasonal cycles ($R^2 = 0.61$ and 0.64 for 90-min- and daily-averaged data), but that SIF signals were more strongly related to downwelling radiation than GPP ($R^2 = 0.91$ for daily-averaged data). The dependence of SIF on radiation obscured the impact of intraseasonal drought in the SIF timeseries, but drought stress was apparent as a decrease in relative SIF, which exhibited a stronger correlation with GPP ($R^2 = 0.56$) than other remotely sensed data over the drought period. These results highlight the potential of SIF for detecting stress-induced losses in forest productivity. Additionally, we found that the red:far-red SIF ratio did not exhibit a response to water stress-induced losses in productivity, but was largely driven by seasonal and interannual changes in canopy structure, as well as by synoptic changes in downwelling radiation.

Plain Language Summary Satellite measurements of solar-induced chlorophyll fluorescence (SIF), a faint light signal emitted from vegetation during photosynthesis, are increasingly being used to estimate ecosystem productivity and carbon uptake. To accurately do so requires a robust understanding of how the relationship between SIF and plant productivity changes over time, in response to environmental stressors, and across different ecosystems. To better understand SIF signals and how they relate to carbon uptake over a temperate deciduous forest, we used a high-precision spectrometer system to observe SIF signals at an AmeriFlux site (US-UMB) in the northern Lower Peninsula of Michigan. While the shared dependence of SIF and ecosystem productivity on sunlight lead to strong daily and seasonal correlations, we found that SIF signals were more closely tied to the amount of incoming sunlight than to ecosystem productivity. Despite the stronger dependence of SIF on sunlight, we show that drought conditions lead to a lower SIF relative to the total light signal. Lastly, we show that the observation of SIF at multiple wavelengths may provide additional information on seasonal and interannual changes in canopy structure. Our results demonstrate the value and limitations in using SIF to assess carbon dynamics over temperate deciduous forest ecosystems.

Key Points:

- Solar-induced chlorophyll fluorescence above a temperate deciduous forest is more strongly tied to radiation than to productivity
- Relative solar-induced fluorescence signals track water stress-induced summer losses in productivity better than absolute fluorescence
- The ratio of red to far-red solar-induced fluorescence is sensitive to phenological changes in canopy structure and downwelling radiation

Supporting Information:

Supporting Information may be found in the online version of this article.

Correspondence to:

Z. Butterfield,
zbutterf@umich.edu

Citation:

Butterfield, Z., Magney, T., Grossmann, K., Bohrer, G., Vogel, C., Barr, S., & Keppel-Aleks, G. (2023). Accounting for changes in radiation improves the ability of SIF to track water stress-induced losses in summer GPP in a temperate deciduous forest. *Journal of Geophysical Research: Biogeosciences*, *128*, e2022JG007352. https://doi.org/10.1029/2022JG007352

Received 19 DEC 2022
Accepted 16 JUN 2023

Author Contributions:

Conceptualization: Zachary Butterfield, Gretchen Keppel-Aleks
Data curation: Zachary Butterfield, Gil Bohrer, Chris Vogel
Formal analysis: Zachary Butterfield
Funding acquisition: Gil Bohrer, Gretchen Keppel-Aleks
Investigation: Zachary Butterfield, Troy Magney, Gretchen Keppel-Aleks
Methodology: Zachary Butterfield, Troy Magney, Katja Grossmann, Gil Bohrer, Gretchen Keppel-Aleks

1. Introduction

Global ecosystems currently provide a sink for roughly one quarter of anthropogenic carbon emissions (Friedlingstein et al., 2022), and the climate-driven variations in this carbon sink therefore have significant implications for long-term changes in climate. Direct quantification of net and gross ecosystem productivity at regional to global scales is elusive, however, given the spatial heterogeneity of the global land surface and the sparse nature of direct observations of land-atmosphere carbon exchange, and contributes significant uncertainty to the global carbon budget (Friedlingstein et al., 2022; Le Quéré et al., 2018).

Project Administration: Gretchen Keppel-Aleks
Resources: Zachary Butterfield, Katja Grossmann, Gil Bohrer, Chris Vogel, Stephen Barr
Software: Zachary Butterfield, Katja Grossmann, Stephen Barr
Supervision: Gretchen Keppel-Aleks
Validation: Zachary Butterfield
Visualization: Zachary Butterfield
Writing – original draft: Zachary Butterfield, Gil Bohrer, Gretchen Keppel-Aleks
Writing – review & editing: Zachary Butterfield, Troy Magney, Katja Grossmann, Gil Bohrer, Gretchen Keppel-Aleks

The unique challenges involved in quantifying biospheric carbon fluxes at the global scale underscore the need for satellite-based observations, as these measurements span a variety of ecosystems and spatiotemporal scales. Terrestrial primary productivity, specifically, has traditionally been quantified using optical indices such as the normalized difference vegetation index (NDVI; Tucker, 1979). These signals represent the "greenness" of vegetation which relates to the amount of light absorbed by leaves, and empirically correlate with productivity across spatial gradients. Solar-induced chlorophyll fluorescence (SIF) is a newer space-based proxy for terrestrial photosynthesis that is directly related to activity in the photosynthetic machinery of vegetation (Frankenberg, Butz, et al., 2011). As leaves absorb solar photons for use in photosynthesis, photons not used for photochemistry are either dissipated as heat via non-photochemical quenching (NPQ) or are fluoresced back to the environment as SIF, which represents an emission of red and far-red photons from the photosystems. Satellite observations of far-red SIF have been shown to scale with spatial and seasonal patterns of gross primary productivity (GPP; Frankenberg, Fisher, et al., 2011; Gao et al., 2021; Li et al., 2018; Sun et al., 2017, 2018), indicating a potential for SIF as a direct proxy of carbon uptake through photosynthesis. There has been a recent proliferation of satellite-based observations of far-red SIF (Frankenberg et al., 2014; Joiner et al., 2013; Köhler et al., 2018) and, more recently, red SIF (Köhler et al., 2020; Wolanin et al., 2015). Quantitative assessments of SIF signals across a range of ecosystems and spatial and temporal scales are needed to inform the interpretation of these data.

The strong relationship between SIF and GPP stems in part from a shared dependence on solar radiation (Magney et al., 2020). Top-of-canopy SIF can be expressed as:

$$\mathrm{SIF} = \mathrm{PAR} \times f\mathrm{PAR} \times \mathrm{SIF}_{\mathrm{yield}} \times f_{\mathrm{esc}} \quad (1)$$

(Zeng et al., 2019) where fluorescence yield ($\mathrm{SIF}_{\mathrm{yield}}$) represents the efficiency at which the photosystems emit photons, photosynthetically active radiation (PAR) indicates downwelling radiation available for photosynthesis, and fPAR indicates the fraction of PAR absorbed by the canopy, which depends primarily on green leaf area, chlorophyll content, and canopy structure. The fluorescence escape ratio (f_{esc}) represents the fraction of total emitted fluorescence that escapes the top of the canopy and can be detected remotely, rather than being deflected or reabsorbed by leaves deeper within the canopy (Dechant et al., 2020; Zeng et al., 2019). Similarly, GPP can be expressed as the product of PAR, fPAR, and light use efficiency (LUE; X. Yang et al., 2015):

$$\mathrm{GPP} = \mathrm{PAR} \times f\mathrm{PAR} \times \mathrm{LUE} \quad (2)$$

LUE, or the efficiency at which sunlight is used to drive photochemistry and carbon fixation (Running et al., 2004), is the most difficult component of GPP to estimate using remote sensing and is traditionally inferred from models (Gitelson & Gamon, 2015; Monteith, 1977). There is, therefore, much interest in characterizing its relationship with SIF (and $\mathrm{SIF}_{\mathrm{yield}}$, or the rate at which absorbed photons are fluoresced as SIF). X. Yang et al. (2015) showed that SIF contained some information about LUE over a temperate deciduous forest, by dividing tower-based SIF by total absorbed PAR to reveal a weak correlation between LUE and $\mathrm{SIF}_{\mathrm{yield}}$, although this relationship was weaker than the correlation between far-red SIF and GPP.

Magney, Bowling, et al. (2019) and Pierrat et al. (2022) further showed a strong relationship between SIF and GPP in northern evergreen forests under minimal changes in canopy structure and absorbed PAR, when more traditional observations such as NDVI, which are closely tied to changes in chlorophyll content, did not capture seasonal productivity dynamics. The demonstrated seasonality in SIF, even when greenness remains constant, suggests that the SIF signal is sensitive to seasonal changes in photoprotective pigments and LUE, and therefore provides a more robust proxy of GPP than greenness alone.

Despite the strong correlations reported between SIF and GPP at seasonal and diurnal timescales, uncertainties remain in the mechanistic relationship between SIF and GPP (Ryu et al., 2019), and in how that relationship changes across different ecosystems and spatiotemporal scales. Several studies have found that SIF over cropland is more closely tied to absorbed PAR (APAR) than to GPP (Miao et al., 2018; K. Yang et al., 2018; Yazbeck et al., 2021), and Zeng et al. (2019) broadly demonstrated that SIF is strongly influenced by canopy structure and changes in f_{esc}. SIF is also dependent on the fluorescence yield of the photosystems, which can itself be influenced by light and biological conditions (Baker, 2008), further complicating its relationship with GPP. Furthermore, while GPP is sensitive to ecosystem stress through changes in LUE, it is not understood how fluorescence yield, and therefore observed SIF, responds to stress-induced changes (Sun et al., 2015). It is therefore unclear how closely the SIF response to environmental stressors mirrors changes in GPP. Several satellite-based studies

have used SIF to observe the impacts of moderate to severe drought in both temperate (Li et al., 2020; Smith et al., 2020; Song et al., 2018; Sun et al., 2015; Yoshida et al., 2015) and tropical regions (Koren et al., 2018; Liu et al., 2017); nonetheless, observations of SIF tend to be less sensitive to interannual variability in GPP during summer and may not show the impacts of mild stress (Butterfield et al., 2020). Furthermore, Yazbeck et al. (2021) demonstrated that SIF did not reliably capture daily-scale reductions in GPP due to water stress at multiple flux tower sites. Wohlfahrt et al. (2018) showed that local scale observations of SIF over a Mediterranean pine forest decoupled from GPP under environmental stress and suggested that much of the strong correlation between SIF and GPP in this ecosystem was driven by a shared dependence on APAR, calling into question the detectability of stress-induced changes in GPP from SIF observations. However, they also noted an increase in the red:far-red SIF ratio aligning with peak stress conditions. The differing behaviors of red and far-red SIF signals during an ecosystem stress event warrant further investigations into what can be learned from simultaneous observations of SIF at both red and far-red wavelengths.

To assess the relationship between SIF and GPP and their responses to environmental variables and stressors, we deployed a tower-based PhotoSpec spectrometer system (Grossmann et al., 2018) above a temperate deciduous forest within the footprint of the US-UMB flux tower at the University of Michigan Biological Station. We present results from 2 years of growing-season observations from late May through October, during which we collected red and far-red SIF observations at a high temporal frequency (~20 s), providing an opportunity to quantify diurnal and intraseasonal variation in the SIF signal. Our goals were to: (a) explore the dependence of SIF on downwelling PAR and test how this dependence influenced the ability of SIF to track intraseasonal changes in GPP; (b) characterize the relationship between SIF and GPP and test how it changed over the course of the growing season and during periods of water stress; and (c) explore the behavior of the red:far-red SIF ratio and assess its response to changes in environmental conditions.

2. Data and Methods

2.1. Study Location at University of Michigan Biological Station

We obtained data at the University of Michigan Biological Station site within a deciduous broadleaf forest composed primarily of aspen, oak, maple, beech, and some understory pine, with a canopy height of approximately 22 m. The forest age is roughly one century as widespread fires burned much of the region in the early twentieth century. The site is characterized by sandy soil, with rapid percolation of rainfall to deep soil layers. This location was chosen in part because it is a well-studied forest ecosystem, with long-standing eddy covariance (EC)-based observations of water and carbon fluxes (Frasson et al., 2015; Gough et al., 2013, 2022), canopy structure (Fotis et al., 2018), soil moisture (He et al., 2014), and sap flow and tree hydrology (Aron et al., 2019; Matheny et al., 2014, 2017).

2.2. PhotoSpec Tower-Based Observations

We built and deployed a PhotoSpec spectrometer system (Grossmann et al., 2018) at the US-UMB tower during the 2018 and 2019 growing seasons (Butterfield et al., 2022). The PhotoSpec system consisted of two narrowband spectrometers (QEPro, Ocean Optics Inc.): one with a wavelength range of 670–732 nm and a resolution of 0.074 nm/pixel, 0.3 nm full width half maximum (FWHM), for measuring SIF in the red region of the spectrum, and a second QEPro (729–784 nm, 0.067 nm/pixel, 0.3 nm FWHM) optimized for measuring SIF in the far-red. An additional broadband spectrometer (Flame, Ocean Optics Inc.; 177–874 nm, 0.382 nm/pixel, 1.2 nm FWHM) permitted the calculation of vegetation indices, such as NDVI, from the measured spectra. A 2-D scanning telescope was mounted on the US-UMB tower at a height of 45 m allowing for the collection of observations from various locations in the canopy using a narrow field of view (about 0.7°). Light from the canopy was thus directed through a fiber optic cable, and subsequently split as input to the three spectrometers.

We acquired automated observations in three azimuthal directions: 60° east of south, due south, and 60° west of south. For each azimuth angle, we acquired data along an elevation transect by scanning from 90° (nadir) to 45° below the horizon. For each individual location along the transects, we optimized the exposure times for the spectrometers to maintain consistent detector signal level. Multiple exposures were then integrated together into 20 s measurements before moving the telescope to the next location. Observations were collected when the solar elevation angle was >10° and solar reference spectra were collected at least every 10 measurements using

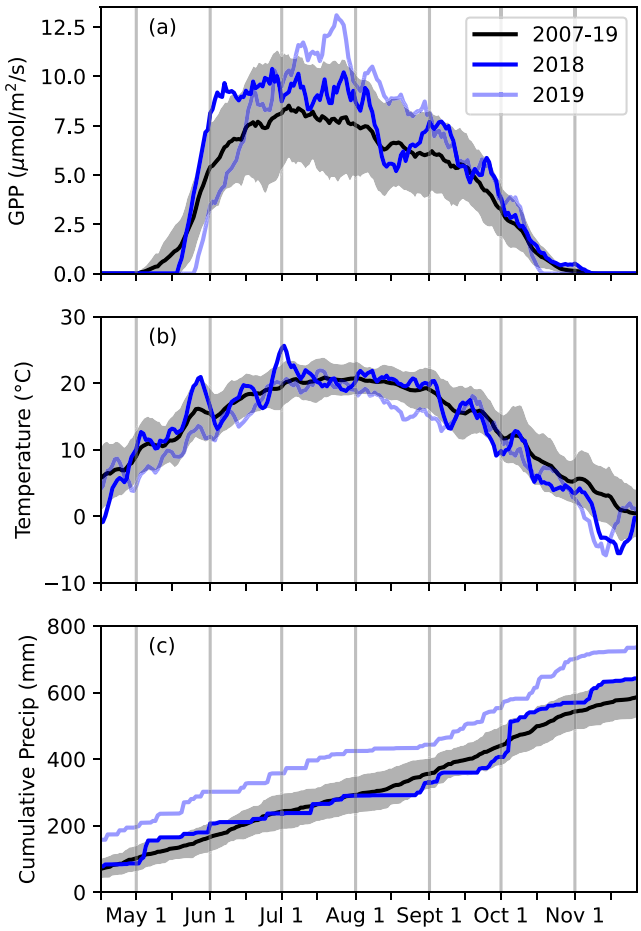

Figure 1. Eddy covariance observations of gross primary productivity (GPP) (a), temperature (b), and cumulative precipitation (c) at US-UMB during the 2018 (dark blue) and 2019 (light blue) growing seasons. The 2007–2019 multi-year mean for each panel is included as a black line, with shading representing ±1 standard deviation. GPP and temperature are plotted as 7-day running means.

an upward-facing diffuser disk. To ensure that observations included green vegetation and were of sufficiently high quality, data were further filtered to only include retrievals where NDVI was >0.2, red and far-red SIF retrieval errors were <0.1 mW m^{-2} sr^{-1} nm^{-1}, and where calculated SIF values fell between −0.1 and 10 mW m^{-2} sr^{-1} nm^{-1} and between −2 and 20% of the total light signal. These filters resulted in the removal of ∼12% of collected data. Rejected data were generally collected under low light level conditions due to low solar zenith angle or gaps in the canopy (Figure S1 in Supporting Information S1), as well as cloudy conditions. A full cycle through the three azimuth angles took approximately 90 min; therefore, after removing outlier data, we used 90-min averages for sub-daily comparisons. The uncertainty of each 90-min period was calculated as the standard deviation of included observations.

SIF radiances were calculated from the QEPro spectra for both the red (680–686 nm) and far-red (745–758 nm) regions of the electromagnetic spectrum using a physical retrieval based on the infilling of solar Fraunhofer lines (Grossmann et al., 2018). To isolate SIF signals from their dependence on PAR, we calculated relative SIF by dividing the observed SIF radiance by the total reflected and fluoresced radiance at the respective wavelength, thus representing SIF as a percentage of the total light signal (Sun et al., 2018). We calculated NDVI, the photochemical reflectance index (PRI), which is sensitive to de-epoxidation of xanthophyll cycle pigments and light use efficiency (Gamon et al., 2001), and a chlorophyll index ($Chlorophyll_{RS}$; Magney, Frankenberg, et al., 2019; Datt, 1999) using spectra from the broadband Flame spectrometer (Text S1 in Supporting Information S1). While our site did not include direct observations of fPAR, which typically require a network of under-canopy PAR sensors, we assumed a rough proportionality between NDVI and fPAR (Running et al., 2004) from which we inferred the qualitative seasonal behavior of fPAR (i.e., we assumed that seasonal changes in fPAR tracked seasonal changes in NDVI).

The SIF observations were radiometrically calibrated using a second broadband Flame spectrometer with a cosine corrector (CC-3-UV-S, Ocean Optics Inc.) that was calibrated using a radiometric standard lamp (HL-3-P-CAL, Ocean Optics Inc.). We recorded simultaneous measurements alongside the PhotoSpec instrument with the second Flame spectrometer using a reflective calibration disk (Spectralon Diffuse Reflectance Standard, Labsphere Inc.) at least once per growing season whenever any adjustments were made to the optical components. Between the 2018 and 2019 growing seasons, radiometric calibration coefficients remained within 2.5% and 1% for red and far-red SIF retrievals, respectively. Wavelength calibrations were done using a Mercury-Argon lamp (HG-1, Ocean Optics Inc.).

2.3. AmeriFlux and Meteorological Data

For this study, we compared PhotoSpec SIF data with ecosystem flux observations from the AmeriFlux tower (46 m above ground), from which CO_2 and H_2O flux data have been observed since 1999 (Gough et al., 2022). EC flux observations of net ecosytem exchange were partitioned into estimates of ecosystem respiration and GPP, from which we used the processed half-hourly estimates of GPP from April 2018 through November 2019 (Figure 1). We used the data from 2007 to 2019 for a baseline comparison with a multi-year mean. In addition to GPP flux data, we used coincident meteorological observations from the same AmeriFlux data set. These included air temperature, precipitation, vapor pressure deficit (VPD), volumetric soil water content (SWC) at a depth of 30 cm, and downwelling PAR. Data for the site was obtained through the AmeriFlux database (AmeriFlux site ID: US-UMB; Gough et al., 2022). More details about the data processing approach for this site are described by Gough et al. (2013) and Text S2 in Supporting Information S1 (see also Lasslop et al., 2010; Morin

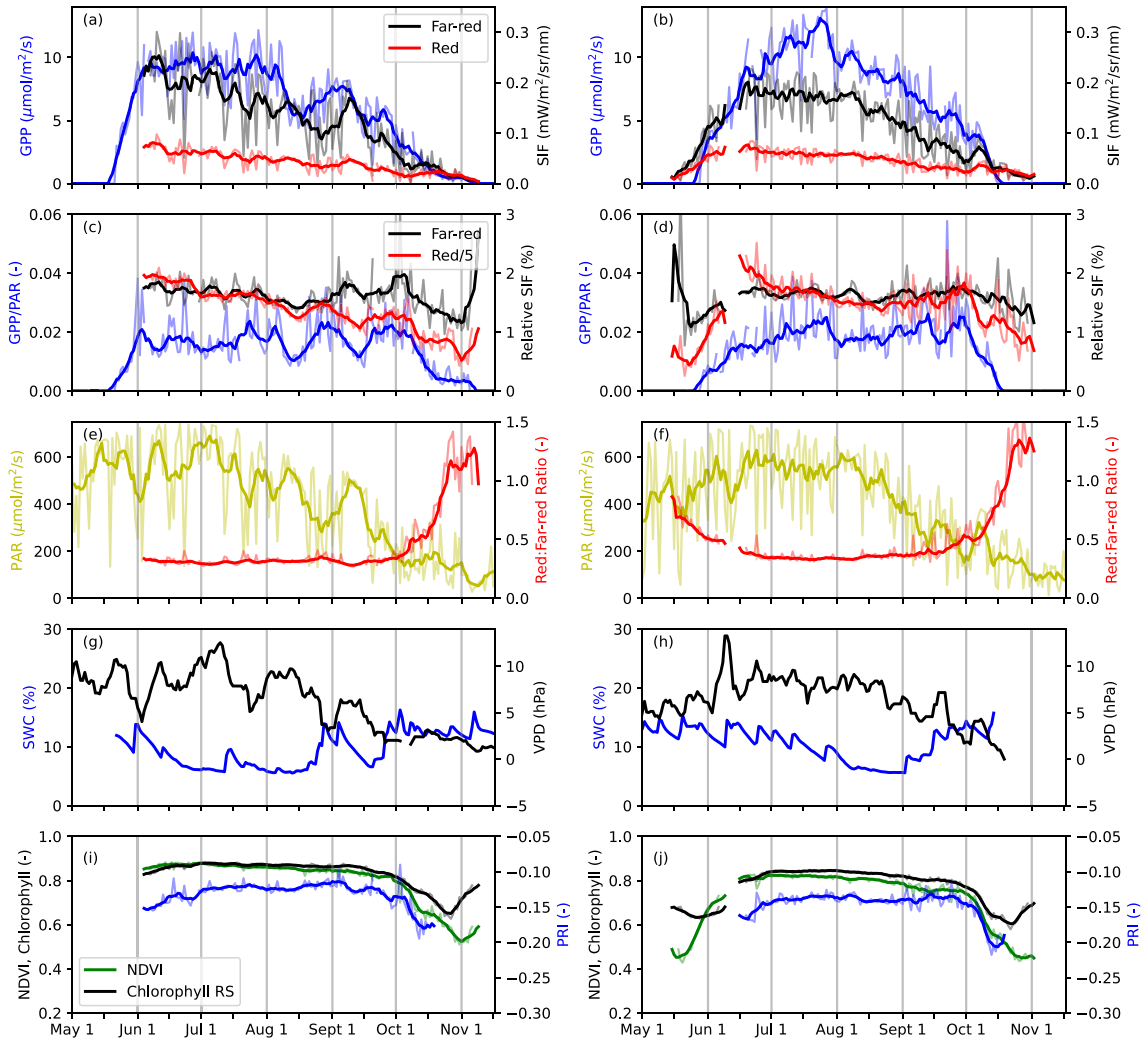

Figure 2. Growing season time series of gross primary productivity (GPP) and SIF radiances (a, b), GPP/PAR and relative SIF (c, d), photosynthetically active radiation (PAR) and the red:far-red SIF ratio (e, f), soil water content (SWC) and vapor pressure deficit (VPD) (g, h), and NDVI, Chlorophyll$_{RS}$, and photochemical reflectance index (i, j) during 2018 (left) and 2019 (right). With the exception of SWC and VPD, bold lines represent the 7-day running mean of daily-averaged data (thin lines). Relative red SIF in panels c and d are divided by 5.

et al., 2014; Rebmann et al., 2012; Reichstein et al., 2005). We aggregated the half-hourly AmeriFlux data to 90-min and daily values.

Because we did not observe fPAR, we assumed that fPAR was near constant under peak growing season conditions from late June through early September when NDVI was stable (Figures 2i and 2j; see Running et al., 2004), and that the relationship during summer between SIF and PAR was therefore indicative of the relationship between SIF and APAR.

As NDVI (and therefore fPAR) was generally constant between leaf out and senescence, we calculated an LUE proxy as GPP/PAR (Gitelson & Gamon, 2015). Seasonal estimates for species-specific maximal leaf area index (LAI) at the site were calculated by collecting litterfall samples with leaf litter traps and subsequently identifying and measuring collected leaves in the lab.

2.4. Satellite Observations of SIF From OCO-2

We compared satellite-based observations of SIF from the Orbiting Carbon Observatory-2 (OCO-2; OCO-2 Science Team et al., 2017; Yu et al., 2019) with our tower-based PhotoSpec observations. OCO-2 is a polar

orbiting satellite with a local overpass time of 1:30p.m. and a footprint of 1.3 × 2.25 km. SIF was retrieved from OCO-2 spectra at 757 and 771 nm using a non-linear least-squares approach to evaluate the infilling of solar Fraunhofer lines (Sun et al., 2018). We used OCO-2 SIF retrievals at 757 nm (which was within our far-red fitting window of 745–758 nm) that fell within a one-degree grid cell centered at US-UMB. Individual soundings were converted to daily-averages using a clear-sky PAR proxy, which uses the cosine of the solar zenith angle to account for diurnal variability in the SIF signal (see Frankenberg, Fisher, et al., 2011; Köhler et al., 2018). For each day with at least 10 individual soundings, we subsequently calculated a mean and standard deviation of OCO-2 observations. This resulted in eight individual data points throughout the 2018 and 2019 growing seasons, each based on an average of ∼140 individual soundings. We then tested the linear correlation of these data with corresponding daily means observed using the PhotoSpec instrument to see how our local observations compared to regional patterns in the SIF signal.

3. Results and Discussion

3.1. 2018–2019 Observations and Climatological Context

Comparison with previous years' EC GPP data showed that the 2018 and 2019 growing seasons were generally more productive than the 2007–2019 mean, with the exceptions of August 2018 and spring 2019 (Figure 1a). In 2018, growing season onset was delayed by about a week relative to the multi-year mean, but GPP increased rapidly (∼0.5 μmol m^{-2} s^{-1} day^{-1}) throughout the second half of May during a period with above average temperatures (Figures 1a and 1b). GPP reached a seasonal peak value of about 10 μmol m^{-2} s^{-1} in late June, roughly 25% higher than the multi-year mean, and remained higher than average until mid-August. In 2019, onset of the growing season occurred even later, lagging the multi-year mean by about 2 weeks, likely due to very wet and cold spring conditions (Figures 1b and 1c). GPP subsequently reached a peak value of >12 μmol m^{-2} s^{-1} day^{-1} in late July, 50% higher than the multi-year mean, and remained nearly a standard deviation higher than average until September (Figure 1a).

Both 2018 and 2019 experienced water stress-induced declines in GPP during late summer that occurred with moderate to severe drought conditions as classified by the U. S. Drought Monitor (USDM; Svoboda et al., 2002; accessed via http://droughtmonitor.unl.edu). The USDM classification showed a severe drought in mid-August 2018 that followed a series of three dry spells in early June, early July, and August (Figure 1c). While the first of these dry periods did not lead to dry soil moisture conditions, the cumulative influence of the two later dry periods led to soil water content falling to ∼5% and coincided with local maxima in VPD upwards of 9 hPa (Figure 2g). Gross primary productivity levels were relatively robust during the first period of dry soil conditions from late June through July 11, but during the second dry period from late July through August 18, productivity ultimately declined by about 30%, to levels below the multi-year mean. Toward the end of August, GPP recovered back to about 20% above the climatological mean. GPP may be increasingly sensitive to dry soil conditions over the growing season due to the fact that the soil matric potential can continue to increase even as SWC asymptotes to a lower limit (Köcher et al., 2009; Lascano et al., 2007). The soil matric potential reflects soil hydraulic tension, which at higher values indicates greater resistance to vegetation taking up water through their roots. Late summer declines in GPP occur roughly every other year at the US-UMB site and are not always tied to an obvious drought signal (Figure S2 in Supporting Information S1). While 2019 was not characterized by any periods of severe drought stress, GPP observations did decrease in late July from about 50% to only 20% above the climatological mean (Figure 1a). This decline in productivity coincided with decreasing SWC (Figure 2h) and low precipitation (Figure 1c), but also with cooler temperatures (Figure 1b) and only a slight increase in VPD (Figure 2h).

PhotoSpec far-red SIF followed a seasonal cycle similar to that of GPP during the 2018 and 2019 growing seasons (Figures 2a and 2b). Both SIF and GPP reached peak levels in July and declined throughout late summer and fall. The red SIF signal followed a similar pattern but exhibited relatively higher values in early spring and fall (Figures 2a and 2b), resulting in higher red:far-red SIF ratios during the shoulder seasons (Figures 2e and 2f) corresponding with low NDVI, $Chlorophyll_{RS}$, and PRI values (Figures 2i and 2j). As discussed further in Section 3.4, SIF signals shared similar temporal patterns with PAR throughout summer months (Figure 2a-2b, e-f). Relative SIF, or SIF as a fraction of the total light signal, was decoupled from the dependence of SIF on PAR (Figures 2c and 2d), as is discussed further in Section 3.4. From late June through September, relative far-red SIF typically was just under 2% of total observed light, while relative red SIF was 5%–10%. While top-of-canopy red SIF was lower than far-red SIF due to greater absorption of red light within the canopy, relative far-red SIF

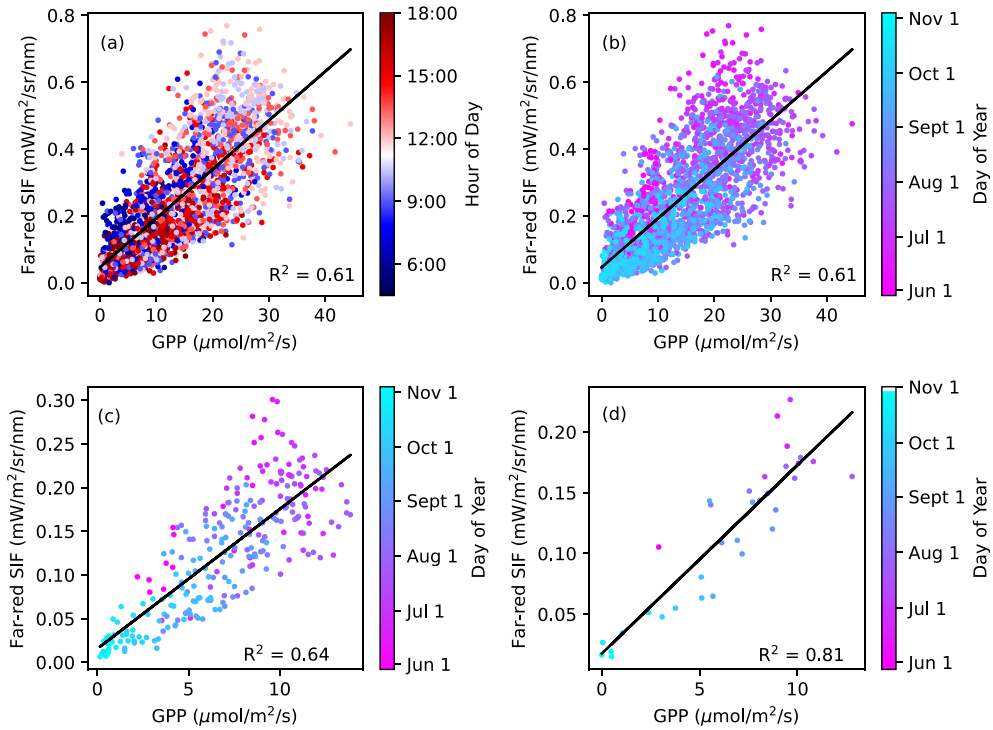

Figure 3. Correlation between far-red SIF and gross primary productivity, temporally aggregated to 90-min (a, b), daily (c), and weekly (d) resolutions. Color bars indicate hour of day (a) or day of year (b–d).

was lower due to the much higher canopy reflectance at far-red wavelengths (Grossmann et al., 2018). Red and far-red relative SIF exhibited lower values during early spring and late fall, when the ecosystem absorbs less downwelling radiation for photosynthesis. We found that relative red SIF and, to some extent, relative far-red SIF visually tracked intraseasonal patterns in the LUE proxy calculated as GPP divided by PAR (Figures 2c and 2d), notably during the August 2018 severe drought. A comparison of daily-averaged data confirmed a positive correlation between GPP/PAR and relative SIF ($R^2 = 0.07$ and $R^2 = 0.34$ for far-red and red relative SIF, respectively; Figure S3 in Supporting Information S1).

3.2. Relationships Between SIF, GPP, and PAR

SIF and GPP were highly correlated when aggregated to 90-min, daily, and weekly timescales (Figure 3). For far-red SIF, weekly-aggregated data had the highest correlation with GPP ($R^2 = 0.81$), while 90-min- and daily-aggregated data had R^2 values of 0.61 and 0.64, respectively. The correlations between GPP and red SIF were weaker (R^2 values of 0.56, 0.57, and 0.72 for 90-min, daily, and weekly timescales; Figure S4 in Supporting Information S1). Over the growing season, weekly mean values of far-red SIF ranged from near zero during the early and late growing season to 0.2 mW m^{-2} sr^{-1} nm^{-1} during peak growing season in July (Figure 3d). Daily values, in contrast, ranged from zero to 0.3 mW m^{-2} sr^{-1} nm^{-1} (Figure 3c), suggesting that weekly-aggregated data reduce the influence of day-to-day variations in far-red SIF that result from cloud-driven variability in PAR. Gross primary productivity spanned a range from zero to about 13 μmol m^{-2} s^{-1} day^{-1} in both weekly- and daily-aggregated data, and daily values exhibited a lower coefficient of variation than far-red SIF throughout the summer (Figure S5 in Supporting Information S1; $\sigma/\mu = 0.21$ and 0.25 for daily GPP and far-red SIF values, respectively, during July), indicating that ecosystem productivity may have been less sensitive to variability in light availability.

SIF was more strongly correlated with PAR ($R^2 = 0.91$ and $R^2 = 0.90$ for daily-averaged far-red and red SIF, respectively; Figure 4a; Figure S6 in Supporting Information S1) than it was with GPP at our site ($R^2 = 0.64$ and $R^2 = 0.57$ for far-red and red SIF; Figure 3c; Figure S4c in Supporting Information S1). While both SIF and GPP depend on PAR and fPAR (Equations 1 and 2), GPP was less tightly coupled to PAR ($R^2 = 0.52$; Figure 4b).

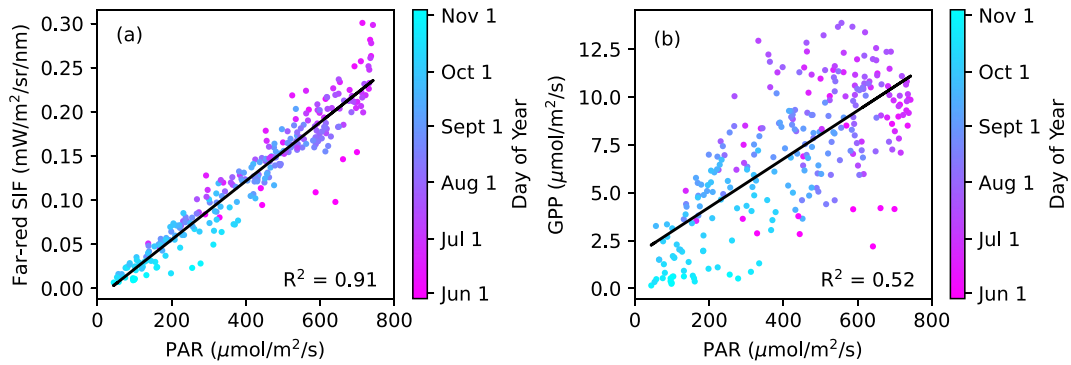

Figure 4. Correlation between daily-averaged far-red SIF (a) and gross primary productivity (b) with photosynthetically active radiation (PAR). Color bars are weighted by day of year.

The higher correlation between SIF and PAR suggests that variations in SIF are dominated by PAR and may not reflect intraseasonal variations in productivity while canopy structure and thus fPAR remain stable. Further, the differential response to fPAR between SIF and GPP complicates the detection of changes in LUE from SIF. Our results contrast with the findings of X. Yang et al. (2015) who found only slightly weaker correlations between SIF and GPP than between SIF and APAR at US-Ha1. US-Ha1 is, however, more radiation-limited than is US-UMB (Wozniak et al., 2020), which could explain a closer coupling between variations in radiation and GPP at their site. Our results are in line with those of K. Yang et al. (2018), who found that SIF is more closely tied to APAR than of GPP over a rice paddy. The different relationships among SIF, GPP, and PAR in these three studies indicate that SIF-derived estimates of productivity may require additional inputs, such as meteorological conditions that may signal ecosystem stress (as have been used for NDVI-derived estimates of GPP; see Running et al., 2004), but also that the necessity of these additional inputs is likely influenced by whether ecosystem productivity is limited by water, temperature, or radiation. However, our findings overall support many studies that have demonstrated that GPP can be estimated from SIF observations from either satellite (Guanter et al., 2012; Sun et al., 2017) or tower (Magney, Bowling, et al., 2019; Pierrat et al., 2022; X. Yang et al., 2015), primarily based on the shared dependence of both SIF and GPP on APAR (Wohlfahrt et al., 2018; K. Yang et al., 2018).

3.3. Seasonal Impacts on the Correlation of SIF With GPP

The relationship between GPP and far-red SIF varies seasonally, as shown by linear correlations of data within individual months for 2018 and 2019 (Figure 5). Linear fits of 90-min data were better constrained to the origin by including near-zero values in morning and evening (when solar zenith angle was low), resulting in more precise slopes (Figure 5a) compared to fits using daily averages (Figure 5c), and consistently stronger correlations throughout the summer (Figure 5b). These results showed that the far-red SIF:GPP slope was highest during the spring at nearly 0.025 (mW m^{-2} sr^{-1} nm^{-1})/(μmol m^{-2} s^{-1}) in May, and declined over the course of the growing season to around 0.015 (mW m^{-2} sr^{-1} nm^{-1})/(μmol m^{-2} s^{-1}) (Figure 5a). Slopes between daily-averaged SIF and GPP typically ranged between 0.01 and 0.02 (mW m^{-2} sr^{-1} nm^{-1})/(μmol m^{-2} s^{-1}), with July 2019 as an outlier (Figure 5c), and the R^2 values were typically higher during spring and fall than mid summer (Figure 5d). The larger uncertainties and lower R^2 values in the monthly relationships between daily-averaged SIF and GPP resulted from these data having smaller coefficients of variation ($\sigma/\mu < 0.3$ in July and August) than 90-min data ($\sigma/\mu > 0.5$ across all months; Figure S5 in Supporting Information S1), although this is less pronounced during spring and fall when phenological changes in the deciduous forest result in a large dynamic range in fPAR (using NDVI as a proxy).

The linear slope between 90-min far-red SIF and GPP decreased over the course of the growing season (Figure 5a), illustrating seasonal variability in the relationship between the two. While a seasonally changing relationship between SIF and productivity has been noted in previous studies (e.g., K. Yang et al., 2018), these studies occurred over cropland where such changes could be attributed to structural changes among different phenological stages. We see the largest month-to-month decline in the linear relationship between far-red SIF and GPP during spring, when there is rapid structural change, but the SIF:GPP relationship above the temperate deciduous forest continues to evolve even after the emergence of a well-developed canopy. The higher SIF:GPP

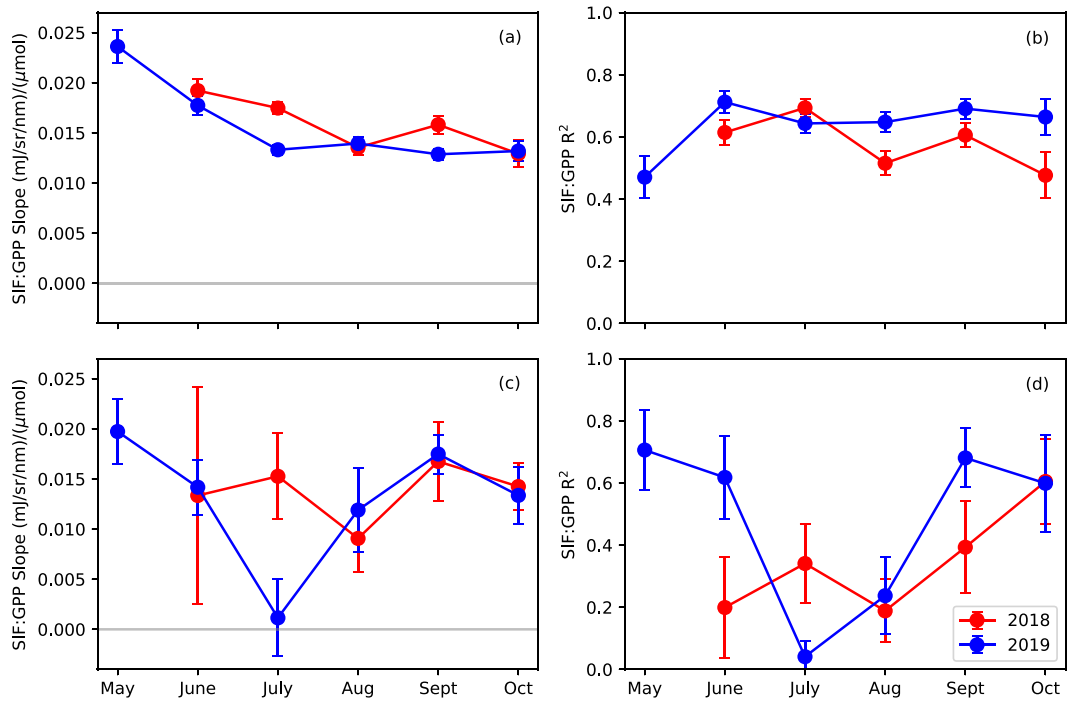

Figure 5. Slopes and R^2 values from monthly linear regressions of 90-min- (a, b) and daily-averaged (c, d) far-red SIF with gross primary productivity. Data from 2018 are in red, while 2019 data are in blue. Error bars represent the standard deviations resulting from calculating slopes and R^2 values using a bootstrapping approach in which we sampled data within a given month with replacement, thus indicating the robustness of the linear regressions.

slope in spring suggests that assuming constant proportionality in scaling SIF to GPP may lead to an overestimate of productivity in springtime, or an underestimate in fall. Butterfield et al. (2020) showed that interannual variability in satellite-based SIF observations is higher in spring and is in better agreement with optical vegetation indices, whereas IAV in fall SIF is smaller and only weakly correlated with other remote sensing products. The seasonal decline in the SIF:GPP relationship could partly explain this phenomenon since it suggests that late-season observations are characterized by a lower SIF signal (and thus a lower signal-to-noise ratio) than are spring data for similar values of GPP, potentially obscuring IAV. The decrease in the SIF:GPP slope as the growing season progresses (Figure 5a) may be due to leaf age effects that impart subtle changes in the canopy. Specifically, if leaves wilt or shrivel as they age due to progressive water stress, absorption of PAR may shift slightly deeper into the canopy where f_{esc} is lower, thus leading to lower top-of-canopy SIF. In the future, observations of leaf area and angle distribution over the course of the growing season, in combination with canopy radiative transfer modeling, may help to further elucidate the drivers of seasonal changes in the SIF:GPP slope.

3.4. Detectability of Mid-Summer Ecosystem Stress

UMBS PhotoSpec SIF observations did not exhibit an obvious response to intraseasonal ecosystem stress dynamics. During August 2018, there were stress-induced decreases in GPP inferred from EC (Figure 2a; Section 3.1) coinciding with severe drought as classified by USDM (Svoboda et al., 2002; accessed via http://droughtmonitor.unl.edu). Linearly detrended summer observations (between July 15 and 15 September 2018) showed that GPP started to decline around August 10 and recovered roughly 20 days later (Figure 6a). However, red and far-red SIF radiances followed synoptic-scale patterns in downwelling PAR, exhibiting higher (instead of lower) values over these 20 relatively cloud- and precipitation-free days (Figures 6a and 6c). Like GPP, far-red and red relative SIF values both showed a local minimum during the drought (between August 14–18; Figure 6b). Primary Component Analysis of the detrended data during this period confirmed that SIF observations remained consistent with (parallel to) PAR and that only relative red and far-red SIF (and, to some extent, PRI) showed changes consistent with the drought-induced declines in GPP and GPP/PAR (Figure S7 in Supporting Information S1). Linear correlations between GPP and other variables during this period revealed that relative far-red SIF was the only variable

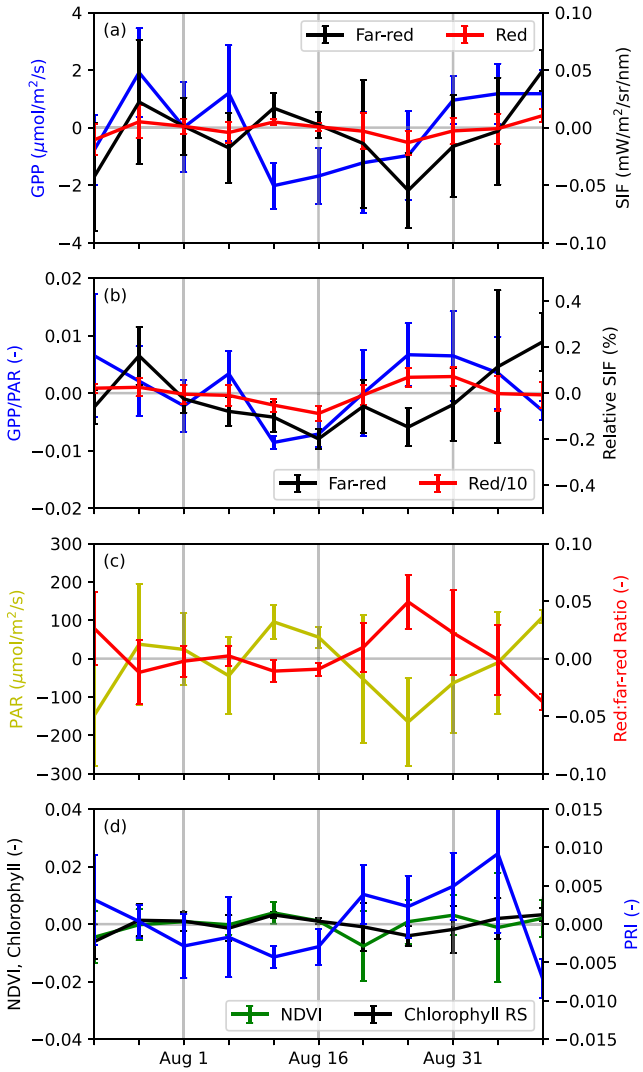

Figure 6. Five-day binned and detrended data showing gross primary productivity (GPP) and SIF radiances (a), GPP/PAR and relative SIF (b), the red:far-red SIF ratio and PAR (c), and NDVI, Chlorophyll$_{RS}$, and photochemical reflectance index (d) over the course of a drought event in August 2018. Error bars represent the standard deviation of each 5-day bin. Tick labels indicate the middle day of each 5-day period. Relative red SIF values in panel b were divided by 10.

to show a statistically significant ($p < 0.01$) relationship with GPP at both daily and 5-day temporal scales (Table S1 in Supporting Information S1).

The decrease in relative SIF values during the August 2018 drought suggests that SIF, when normalized by light levels, may reflect changes in productivity that are independent from APAR. Surprisingly, it was relative *red* SIF values, which did not exhibit a statistically significant correlation with GPP (Table S1 in Supporting Information S1), that showed a strong correlation with GPP/PAR at both daily ($R = 0.69$) and 5-day ($R = 0.87$) temporal scales. In contrast, the relative far-red SIF signals did not exhibit significant correlations with GPP/PAR, our LUE proxy, at daily ($R = -0.17$) or 5-day ($R = 0.08$) scales. While we did not observe any corresponding changes in NDVI and Chlorophyll$_{RS}$ during the August 2018 drought, there was a delayed increase in PRI following the drought by ~10 days (Figure 6) which may indicate an increase in carotenoid pigments resulting from the drought period.

A simple optimized regression model using far-red absolute and relative SIF observations did not significantly improve the ability to capture variations in GPP (Figure S8 in Supporting Information S1). Including both absolute and relative SIF as input variables for the model resulted in only an additional 1% predictive power than when using only far-red SIF (65% variability explained using both absolute and relative SIF, vs. 64% of variability explained using absolute SIF alone; Figure S8 in Supporting Information S1), as relative SIF did not share a similar seasonal pattern with SIF and GPP; weighting relative SIF more strongly allows for better capturing summer drought effects, but worsens the ability of the model to reproduce spring and fall changes in GPP. We note that our model was based on only two seasons of data in a single ecosystem and that a simple regression model did not allow for nonlinear weighting of variables based on limiting factors (i.e., water-limited and radiation/temperature-limited regimes).

The limited response of red and far-red SIF radiances to summer declines in GPP underscores the challenges in using SIF to estimate productivity under stable canopy conditions. Similar to our findings, Wohlfahrt et al. (2018) showed that SIF signals in a Mediterranean pine forest exhibited poor correlation with GPP during a heat wave, although their data indicated that top-of-canopy SIF signals eventually declined in response to losses in productivity. Marrs et al. (2020) also found that SIF signals in individual deciduous species did not exhibit an immediate response to induced water stress. More promising is that we found that relative far-red SIF did somewhat track stress-induced changes in GPP over both daily and 5-day timescales, and that relative red SIF consistently mirrored synoptic-scale changes in GPP/PAR, indicating that SIF observations did capture changes in GPP and LUE when isolated from their dependence on PAR. These results highlight the contrasting information from absolute and relative SIF, in that absolute SIF provides a better proxy for GPP across seasonal and diurnal scales driven that are subject to changes in temperature and PAR, while relative SIF better tracks GPP at intraseasonal scales under water-limited conditions. Future studies should investigate whether ancillary environmental data can, in conjunction with SIF observations, further improve our ability to reproduce variability in GPP across various productivity limiting factors, and explore how these relationships change between different plant types and ecosystems.

3.5. Interpretation of the Red:Far-Red SIF Ratio

The red:far-red SIF ratio did not show a coincident response to drought-induced reductions in GPP (Figures 6a and 6c). Similarly, diurnal stress-induced effects were not evident in the 90-min-aggregated observations of the red:far-red SIF ratio (Figure S9 in Supporting Information S1). Our results corroborated Magney, Frankenberg,

Table 1
Species-Specific Leaf Area Index (LAI) Measured at the US-UMB AmeriFlux Site for 2018 and 2019 Using Leaf Litter Traps

Species	2018 LAI	2019 LAI
Bigtooth aspen (*Populus grandidentata*)	1.286	0.981
Red maple (*Acer rubrum*)	0.891	0.730
American beech (*Fagus grandifolia*)	0.292	0.281
Red oak (*Quercus rubra*)	1.073	0.878
Paper birch (*Betula papyrifera*)	0.238	0.178
White pine (*Pinus strobus*)	0.587	0.578
Red pine (*Pinus resinosa*)	0.008	0.011
Total	4.375	3.636

Note. Total values include all observed tree species.

et al. (2019; see their Figure 7b, our Figure S9 in Supporting Information S1), who showed that although stressed conditions lead to a lower red:far-red ratio at the leaf level, these leaf-level changes in NPQ were not noticeable in canopy-level measurements. We instead found that the detrended daily SIF ratio at our study location was strongly anticorrelated ($R^2 = 0.79$) with PAR during the August 2018 drought (Figure 6c). Control of the SIF ratio by downwelling PAR is in contrast to Wohlfahrt et al. (2018) who observed an increase in the red:far-red SIF ratio in response to heat stress and hypothesized that the contrasting response of SIF at different wavelengths may have been due to a decrease in chlorophyll content.

Because downwelling PAR reaches further into the understory during time periods with a more open canopy, the red:far-red SIF ratio was lower with a fuller canopy at seasonal and interannual scales. We saw higher red:far-red ratios during early spring canopy development, and in late fall as canopy chlorophyll content dropped, similar to Magney, Frankenberg, et al. (2019). During spring and fall, lower leaf area and decreased chlorophyll content reduce reabsorption of red SIF by the canopy, increasing the red:far-red ratio. At interannual scales, the red:far-red SIF ratio was lower in 2018 than in 2019 corresponding with a higher maximum NDVI (0.88 in 2018 vs. 0.84 in 2019) and 20% greater LAI (4.38 in 2018 vs. 3.64 in 2019; Table 1). The lower red:far-red SIF ratio in 2018, when LAI was high, corroborates the hypothesis that a denser canopy limits top-of-canopy red fluorescence. These results highlight the value in simultaneous retrievals of SIF at multiple wavelengths, available from satellite-based instruments such as TROPOMI (Köhler et al., 2020), but also demonstrate that the interpretation of SIF observations at multiple wavelengths must be cognizant of differences in sensitivity to ecosystem and environmental changes on synoptic, seasonal, and interannual timescales. Ultimately, our results demonstrate that further studies into the response of the red:far-red SIF ratio to environmental stress would require a detailed analysis of both the influence of phenological changes in canopy structure as well as incoming light conditions on top-of-canopy SIF observations. These analyses necessitate that observations be made at high temporal frequency since year-to-year or even month-to-month changes are primarily driven by changes in canopy structure that are independent of environmental stress, as well as the incorporation of canopy radiative transfer modeling.

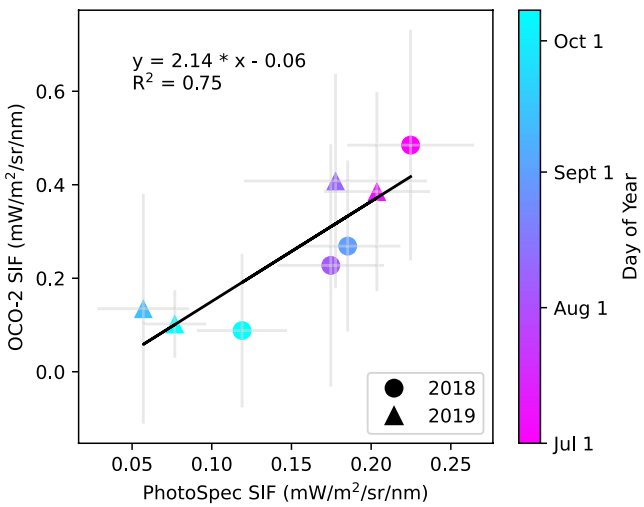

Figure 7. Correlation and linear fit results between far-red SIF observations from PhotoSpec and the OCO-2 satellite. OCO-2 data includes individual days that contained at least 10 soundings within a one-degree gridcell centered at US-UMB. Each sounding was multiplied by a daily correction factor, which uses a clear-sky proxy to account for diurnal changes in the SIF signal, before calculating a daily mean. Error bars represent the standard deviation of included observations. Daily mean values from OCO-2 were then correlated with the daily-average SIF signal from the PhotoSpec instrument, where uncertainties were propagated from the standard deviation of 20 s observations included in every sub-daily 90-min average. Circles indicate data from 2018 and triangles indicate 2019. The color bar is weighted by day of year.

3.6. Comparison With Space-Based SIF From OCO-2

Daily averages of far-red SIF observations from PhotoSpec were significantly correlated with mean estimates of daily-averaged SIF from the OCO-2 satellite ($R^2 = 0.75$, $p < 0.01$; Figure 7). While OCO-2 rarely passed directly over our study location at US-UMB (Figure S10 in Supporting Information S1), these results suggest significant agreement between our instrument and the SIF signal from the surrounding region. The slope between the two datasets was 2.1 ± 0.5, reflecting that the raw SIF radiance measured by OCO-2 was twice that measured by PhotoSpec. The lower radiance values observed by our PhotoSpec instrument likely resulted from the PhotoSpec telescope being deployed on the south side of the tower and collecting observations with a viewing elevation angle of up to 45° below horizon. This sampling pattern often led to larger incident angles between solar and viewing directions, thereby included a greater fraction of shaded vegetation in our observations. These differences highlight that, while tower- and space-based platforms capture similar temporal patterns in SIF signals, more comprehensive comparisons between SIF observations require a more complex study of viewing and illumination angle sensitivities in top-of-canopy SIF observations, as well as careful calibration of individual instruments.

4. Conclusions

We deployed a PhotoSpec system with two high spectral resolution spectrometers for measuring red and far-red SIF to a deciduous forest in northern Michigan. Results from the first 2 years of data acquisition showed that SIF signals over a temperate deciduous forest are more strongly related to radiation than to photosynthetic productivity. While a shared dependence on PAR did result in a significant correlation between SIF and GPP, the slope of this linear relationship gradually decreased over the course of the growing season, indicating that temporal changes in the far-red SIF:GPP ratio should be considered when using SIF to assess ecosystem productivity.

Our study demonstrates challenges in using SIF radiances to detect short-term stress-induced declines in ecosystem productivity. Nonetheless, we showed that observations of relative SIF may be a more reliable indicator of ecosystem stress, indicating that SIF signals do respond to stress-induced changes in productivity and track changes in LUE after accounting for changes in solar radiation. Given contrasting information from absolute and relative SIF values, future studies should explore how to improve the interpretation of SIF observations that span multiple productivity limiting factors. Additionally, we showed that the red:far-red SIF ratio is sensitive to seasonal and interannual changes in canopy structure, as well as downwelling radiation. Our results point to the need for coordinated multi-scale studies on the relationship between SIF and photosynthesis including at the leaf and canopy level, especially under conditions of environmental stress.

Data Availability Statement

SIF and other PhotoSpec data are available at https://doi.org/10.7302/sx8c-y281. AmeriFlux environmental and eddy flux data are available at https://doi.org/10.17190/AMF/1246107. OCO-2 SIF data are available at https://doi.org/10.5067/XO2LBBNPO010.

Acknowledgments
We acknowledge funding for this research provided by NASA Interdisciplinary Science (80NSSC17K0116) and NASA's OCO-2 science team (80NSSC21K1070). Funding for the US-UMB core site was provided by the U.S. Department of Energy's Office of Science. We thank Jochen Stutz and his team at the University of California Los Angeles, as well as Brad Angelocci and Robb Gillespie at the Space Physics Research Laboratory at the University of Michigan, for their assistance with the construction of the PhotoSpec instrument. We also thank two anonymous reviewers for their helpful critique and feedback.

References

Aron, P. G., Poulsen, C. J., Fiorella, R. P., & Matheny, A. M. (2019). Stable water isotopes reveal effects of intermediate disturbance and canopy structure on forest water cycling. *Journal of Geophysical Research: Biogeosciences*, *124*(10), 2958–2975. https://doi.org/10.1029/2019jg005118

Baker, N. R. (2008). Chlorophyll fluorescence: A probe of photosynthesis in vivo. *Annual Review of Plant Biology*, *59*(1), 89–113. https://doi.org/10.1146/annurev.arplant.59.032607.092759

Butterfield, Z., Buermann, W., & Keppel-Aleks, G. (2020). Satellite observations reveal seasonal redistribution of northern ecosystem productivity in response to interannual climate variability. *Remote Sensing of Environment*, *242*, 111755. https://doi.org/10.1016/j.rse.2020.111755

Butterfield, Z., Muccio, D., & Keppel-Aleks, G. (2022). Tower observations of solar-induced chlorophyll fluorescence at the University of Michigan Biological Station [Dataset]. University of Michigan - Deep Blue Data. https://doi.org/10.7302/sx8c-y281

Datt, B. (1999). A new reflectance index for remote sensing of chlorophyll content in higher plants: Tests using Eucalyptus leaves. *Journal of Plant Physiology*, *154*(1), 30–36. https://doi.org/10.1016/S0176-1617(99)80314-9

Dechant, B., Ryu, Y., Badgley, G., Zeng, Y., Berry, J. A., Zhang, Y., et al. (2020). Canopy structure explains the relationship between photosynthesis and sun-induced chlorophyll fluorescence in crops. *Remote Sensing of Environment*, *241*, 111733. https://doi.org/10.1016/j.rse.2020.111733

Fotis, A. T., Morin, T. H., Fahey, R. T., Hardiman, B. S., Bohrer, G., & Curtis, P. S. (2018). Forest structure in space and time: Biotic and abiotic determinants of canopy complexity and their effects on net primary productivity. *Agricultural and Forest Meteorology*, *250*, 181–191. https://doi.org/10.1016/j.agrformet.2017.12.251

Frankenberg, C., Butz, A., & Toon, G. C. (2011). Disentangling chlorophyll fluorescence from atmospheric scattering effects in O_2 A-band spectra of reflected sun-light. *Geophysical Research Letters*, *38*(3), L03801. https://doi.org/10.1029/2010gl045896

Frankenberg, C., Fisher, J. B., Worden, J., Badgley, G., Saatchi, S. S., Lee, J., et al. (2011). New global observations of the terrestrial carbon cycle from GOSAT: Patterns of plant fluorescence with gross primary productivity. *Geophysical Research Letters*, *38*(17), L17706. https://doi.org/10.1029/2011gl048738

Frankenberg, C., O'Dell, C., Berry, J., Guanter, L., Joiner, J., Köhler, P., et al. (2014). Prospects for chlorophyll fluorescence remote sensing from the orbiting carbon observatory-2. *Remote Sensing of Environment*, *147*, 1–12. https://doi.org/10.1016/j.rse.2014.02.007

Frasson, R. P. D. M., Bohrer, G., Medvigy, D., Matheny, A. M., Morin, T. H., Vogel, C. S., et al. (2015). Modeling forest carbon cycle response to tree mortality: Effects of plant functional type and disturbance intensity. *Journal of Geophysical Research: Biogeosciences*, *120*(11), 2178–2193. https://doi.org/10.1002/2015jg003035

Friedlingstein, P., Jones, M. W., O'Sullivan, M., Andrew, R. M., Bakker, D. C. E., Hauck, J., et al. (2022). Global carbon budget 2021. *Earth System Science Data*, *14*(4), 1917–2005. https://doi.org/10.5194/essd-14-1917-2022

Gamon, J. A., Field, C. B., Fredeen, A. L., & Thayer, S. (2001). Assessing photosynthetic downregulation in sunflower stands with an optically-based model. *Photosynthesis Research*, *67*(1–2), 113–125. https://doi.org/10.1023/a:1010677605091

Gao, H., Liu, S., Lu, W., Smith, A. R., Valbuena, R., Yan, W., et al. (2021). Global analysis of the relationship between reconstructed solar-induced chlorophyll fluorescence (SIF) and gross primary production (GPP). *Remote Sensing*, *13*(14), 2824. https://doi.org/10.3390/rs13142824

Gitelson, A. A., & Gamon, J. A. (2015). The need for a common basis for defining light-use efficiency: Implications for productivity estimation. *Remote Sensing of Environment*, *156*, 196–201. https://doi.org/10.1016/j.rse.2014.09.017

Gough, C. M., Bohrer, G., & Curtis, P. (2022). AmeriFlux BASE US-UMB Univ. of Mich. Biological station, ver. 18-5 [Dataset]. AmeriFlux AMP. https://doi.org/10.17190/AMF/1246107

Gough, C. M., Hardiman, B. S., Nave, L. E., Bohrer, G., Maurer, K. D., Vogel, C. S., et al. (2013). Sustained carbon uptake and storage following moderate disturbance in a Great Lakes forest. *Ecological Applications*, *23*(5), 1202–1215. https://doi.org/10.1890/12-1554.1

Grossmann, K., Frankenberg, C., Magney, T. S., Hurlock, S. C., Seibt, U., & Stutz, J. (2018). Remote sensing of environment PhotoSpec: A new instrument to measure spatially distributed red and far-red solar-induced chlorophyll fluorescence. *Remote Sensing of Environment*, *216*(June), 311–327. https://doi.org/10.1016/j.rse.2018.07.002

Guanter, L., Frankenberg, C., Dudhia, A., Lewis, P. E., Gómez-Dans, J., Kuze, A., et al. (2012). Retrieval and global assessment of terrestrial chlorophyll fluorescence from GOSAT space measurements. *Remote Sensing of Environment*, *121*, 236–251. https://doi.org/10.1016/j.rse.2012.02.006

He, L., Ivanov, V. Y., Bohrer, G., Maurer, K. D., Vogel, C. S., & Moghaddam, M. (2014). Effects of fine-scale soil moisture and canopy heterogeneity on energy and water fluxes in a northern temperate mixed forest. *Agricultural and Forest Meteorology*, *184*, 243–256. https://doi.org/10.1016/j.agrformet.2013.10.006

Joiner, J., Guanter, L., Lindstrot, R., Voigt, M., Vasilkov, A. P., Middleton, E. M., et al. (2013). Global monitoring of terrestrial chlorophyll fluorescence from moderate-spectral-resolution near-infrared satellite measurements: Methodology, simulations, and application to GOME-2. *Atmospheric Measurement Techniques*, *6*(10), 2803–2823. https://doi.org/10.5194/amt-6-2803-2013

Köcher, P., Gebauer, T., Horna, V., & Leuschner, C. (2009). Leaf water status and stem xylem flux in relation to soil drought in five temperate broad-leaved tree species with contrasting water use strategies. *Annals of Forest Science*, *66*(1), 1. https://doi.org/10.1051/forest/2008076

Köhler, P., Behrenfeld, M. J., Landgraf, J., Joiner, J., Magney, T. S., & Frankenberg, C. (2020). Global retrievals of solar-induced chlorophyll fluorescence at red wavelengths with TROPOMI. *Geophysical Research Letters*, *47*(15), e2020GL087541. https://doi.org/10.1029/2020gl087541

Köhler, P., Frankenberg, C., Magney, T. S., Guanter, L., Joiner, J., & Landgraf, J. (2018). Global retrievals of solar-induced chlorophyll fluorescence with TROPOMI: First results and intersensor comparison to OCO-2. *Geophysical Research Letters*, *45*(19), 10–456. https://doi.org/10.1029/2018gl079031

Koren, G., Van Schaik, E., Araújo, A. C., Boersma, K. F., Gärtner, A., Killaars, L., et al. (2018). Widespread reduction in sun-induced fluorescence from the Amazon during the 2015/2016 El Niño. *Philosophical Transactions of the Royal Society B: Biological Sciences*, *373*(1760), 20170408. https://doi.org/10.1098/rstb.2017.0408

Lascano, R., Sojka, R. E., & Evett, S. (2007). Soil water and monitoring technology. https://doi.org/10.2134/agronmonogr30.2ed.c2

Lasslop, G., Reichstein, M., Papale, D., Richardson, A. D., Arneth, A., Barr, A., et al. (2010). Separation of net ecosystem exchange into assimilation and respiration using a light response curve approach: Critical issues and global evaluation. *Global Change Biology*, *16*(1), 187–208. https://doi.org/10.1111/j.1365-2486.2009.02041.x

Le Quéré, C., Andrew, R. M., Friedlingstein, P., Sitch, S., Pongratz, J., Manning, A. C., et al. (2018). Global carbon budget 2017. *Earth System Science Data*, *10*(1), 405–448. https://doi.org/10.5194/essd-10-405-2018

Li, X., Xiao, J., He, B., Altaf Arain, M., Beringer, J., Desai, A. R., et al. (2018). Solar-induced chlorophyll fluorescence is strongly correlated with terrestrial photosynthesis for a wide variety of biomes: First global analysis based on OCO-2 and flux tower observations. *Global Change Biology*, *24*(9), 3990–4008. https://doi.org/10.1111/gcb.14297

Li, X., Xiao, J., Kimball, J. S., Reichle, R. H., Scott, R. L., Litvak, M. E., et al. (2020). Synergistic use of SMAP and OCO-2 data in assessing the responses of ecosystem productivity to the 2018 US drought. *Remote Sensing of Environment*, *251*, 112062. https://doi.org/10.1016/j.rse.2020.112062

Liu, J., Bowman, K. W., Schimel, D. S., Parazoo, N. C., Jiang, Z., Lee, M., et al. (2017). Contrasting carbon cycle responses of the tropical continents to the 2015–2016 El Niño. *Science*, *358*(6360), eaam5690. https://doi.org/10.1126/science.aam5690

Magney, T. S., Barnes, M. L., & Yang, X. (2020). On the covariation of chlorophyll fluorescence and photosynthesis across scales. *Geophysical Research Letters*, *47*(23), e2020GL091098. https://doi.org/10.1029/2020gl091098

Magney, T. S., Bowling, D. R., Logan, B. A., Grossmann, K., Stutz, J., Blanken, P. D., et al. (2019). Mechanistic evidence for tracking the seasonality of photosynthesis with solar-induced fluorescence. *Proceedings of the National Academy of Sciences*, *116*(24), 11640–11645. https://doi.org/10.1073/pnas.1900278116

Magney, T. S., Frankenberg, C., Köhler, P., North, G., Davis, T. S., Dold, C., et al. (2019). Disentangling changes in the spectral shape of chlorophyll fluorescence: Implications for remote sensing of photosynthesis. *Journal of Geophysical Research: Biogeosciences*, *124*(6), 1491–1507. https://doi.org/10.1029/2019jg005029

Marrs, J. K., Reblin, J. S., Logan, B. A., Allen, D. W., Reinmann, A. B., Bombard, D. M., et al. (2020). Solar-induced fluorescence does not track photosynthetic carbon assimilation following induced stomatal closure. *Geophysical Research Letters*, *47*(15), e2020GL087956. https://doi.org/10.1029/2020gl087956

Matheny, A. M., Bohrer, G., Vogel, C. S., Morin, T. H., He, L., Frasson, R. P. D. M., et al. (2014). Species-specific transpiration responses to intermediate disturbance in a northern hardwood forest. *Journal of Geophysical Research: Biogeosciences*, *119*(12), 2292–2311. https://doi.org/10.1002/2014jg002804

Matheny, A. M., Fiorella, R. P., Bohrer, G., Poulsen, C. J., Morin, T. H., Wunderlich, A., et al. (2017). Contrasting strategies of hydraulic control in two codominant temperate tree species. *Ecohydrology*, *10*(3), e1815. https://doi.org/10.1002/eco.1815

Miao, G., Guan, K., Yang, X., Bernacchi, C. J., Berry, J. A., DeLucia, E. H., et al. (2018). Sun-induced chlorophyll fluorescence, photosynthesis, and light use efficiency of a soybean field from seasonally continuous measurements. *Journal of Geophysical Research: Biogeosciences*, *123*(2), 610–623. https://doi.org/10.1002/2017jg004180

Monteith, J. L. (1977). Climate and the efficiency of crop production in Britain. *Philosophical Transactions of the Royal Society of London B Biological Sciences*, *281*(980), 277–294.

Morin, T. H., Bohrer, G., Frasson, R. P. D. M., Naor-Azreli, L., Mesi, S., Stefanik, K. C., & Schäfer, K. V. R. (2014). Environmental drivers of methane fluxes from an urban temperate wetland park. *Journal of Geophysical Research: Biogeosciences*, *119*(11), 2188–2208. https://doi.org/10.1002/2014jg002750

OCO-2 Science Team, Gunson, M., & Eldering, A. (2017). *OCO-2 Level 2 bias-corrected solar-induced fluorescence and other select fields from the IMAP-DOAS algorithm aggregated as daily files, Retrospective processing V8r* [Dataset]. Goddard Earth Sciences Data and Information Services Center (GES DISC). https://doi.org/10.5067/AJMZO5O3TGUR

Pierrat, Z., Magney, T., Parazoo, N. C., Grossmann, K., Bowling, D. R., Seibt, U., et al. (2022). Diurnal and seasonal dynamics of solar-induced chlorophyll fluorescence, vegetation indices, and gross primary productivity in the boreal forest. *Journal of Geophysical Research: Biogeosciences*, *127*(2), e2021JG006588. https://doi.org/10.1029/2021jg006588

Rebmann, C., Kolle, O., Heinesch, B., Queck, R., Ibrom, A., & Aubinet, M. (2012). Data acquisition and flux calculations. In *Eddy covariance* (pp. 59–83). Springer.

Reichstein, M., Falge, E., Baldocchi, D., Papale, D., Aubinet, M., Berbigier, P., et al. (2005). On the separation of net ecosystem exchange into assimilation and ecosystem respiration: Review and improved algorithm. *Global Change Biology*, *11*(9), 1424–1439. https://doi.org/10.1111/j.1365-2486.2005.001002.x

Running, S. W., Nemani, R. R., Heinsch, F. A., Zhao, M., Reeves, M., & Hashimoto, H. (2004). A continuous satellite-derived measure of global terrestrial primary production. *AIBS Bulletin*, *54*(6), 547–560. https://doi.org/10.1641/0006-3568(2004)054[0547:acsmog]2.0.co;2

Ryu, Y., Berry, J. A., & Baldocchi, D. D. (2019). What is global photosynthesis? History, uncertainties and opportunities. *Remote Sensing of Environment*, *223*, 95–114. https://doi.org/10.1016/j.rse.2019.01.016

Smith, N. E., Kooijmans, L. M. J., Koren, G., Van Schaik, E., van Der Woude, A. M., Wanders, N., et al. (2020). Spring enhancement and summer reduction in carbon uptake during the 2018 drought in northwestern Europe. *Philosophical Transactions of the Royal Society B*, *375*(1810), 20190509. https://doi.org/10.1098/rstb.2019.0509

Song, L., Guanter, L., Guan, K., You, L., Huete, A., Ju, W., & Zhang, Y. (2018). Satellite sun-induced chlorophyll fluorescence detects early response of winter wheat to heat stress in the Indian Indo-Gangetic Plains. *Global Change Biology*, *24*(9), 4023–4037. https://doi.org/10.1111/gcb.14302

Sun, Y., Frankenberg, C., Jung, M., Joiner, J., Guanter, L., Köhler, P., & Magney, T. (2018). Overview of solar-induced chlorophyll fluorescence (SIF) from the orbiting carbon observatory-2: Retrieval, cross-mission comparison, and global monitoring for GPP. *Remote Sensing of Environment*, *209*, 808–823. https://doi.org/10.1016/j.rse.2018.02.016

Sun, Y., Frankenberg, C., Wood, J. D., Schimel, D. S., Jung, M., Guanter, L., et al. (2017). OCO-2 advances photosynthesis observation from space via solar-induced chlorophyll fluorescence. *Science*, *358*(6360), eaam5747. https://doi.org/10.1126/science.aam5747

Sun, Y., Fu, R., Dickinson, R., Joiner, J., Frankenberg, C., Gu, L., et al. (2015). Drought onset mechanisms revealed by satellite solar-induced chlorophyll fluorescence: Insights from two contrasting extreme events. *Journal of Geophysical Research: Biogeosciences*, *120*(11), 2427–2440. https://doi.org/10.1002/2015jg003150

Svoboda, M., LeComte, D., Hayes, M., Heim, R., Gleason, K., Angel, J., et al. (2002). The drought monitor. *Bulletin of the American Meteorological Society*, *83*(8), 1181–1190. https://doi.org/10.1175/1520-0477-83.8.1181

Tucker, C. J. (1979). Red and photographic infrared linear combinations for monitoring vegetation. *Remote Sensing of Environment*, *8*(2), 127–150. https://doi.org/10.1016/0034-4257(79)90013-0

Wohlfahrt, G., Gerdel, K., Migliavacca, M., Rotenberg, E., Tatarinov, F., Müller, J., et al. (2018). Sun-induced fluorescence and gross primary productivity during a heat wave. *Scientific Reports*, *8*(1), 14169. https://doi.org/10.1038/s41598-018-32602-z

Wolanin, A., Rozanov, V. v., Dinter, T., Noël, S., Vountas, M., Burrows, J. P., & Bracher, A. (2015). Global retrieval of marine and terrestrial chlorophyll fluorescence at its red peak using hyperspectral top of atmosphere radiance measurements: Feasibility study and first results. *Remote Sensing of Environment*, *166*, 243–261. https://doi.org/10.1016/j.rse.2015.05.018

Wozniak, M. C., Bonan, G. B., Keppel-Aleks, G., & Steiner, A. L. (2020). Influence of vertical heterogeneities in the canopy microenvironment on interannual variability of carbon uptake in temperate deciduous forests. *Journal of Geophysical Research: Biogeosciences*, *125*(8), e2020JG005658. https://doi.org/10.1029/2020jg005658

Yang, K., Ryu, Y., Dechant, B., Berry, J. A., Hwang, Y., Jiang, C., et al. (2018). Sun-induced chlorophyll fluorescence is more strongly related to absorbed light than to photosynthesis at half-hourly resolution in a rice paddy. *Remote Sensing of Environment*, *216*, 658–673. https://doi.org/10.1016/j.rse.2018.07.008

Yang, X., Tang, J., Mustard, J. F., Lee, J., Rossini, M., Joiner, J., et al. (2015). Solar-induced chlorophyll fluorescence that correlates with canopy photosynthesis on diurnal and seasonal scales in a temperate deciduous forest. *Geophysical Research Letters*, *42*(8), 2977–2987. https://doi.org/10.1002/2015gl063201

Yazbeck, T., Bohrer, G., Gentine, P., Ye, L., Arriga, N., Bernhofer, C., et al. (2021). Site characteristics mediate the relationship between forest productivity and satellite measured solar induced fluorescence. *Frontiers in Forests and Global Change*, *193*. https://doi.org/10.3389/ffgc.2021.695269

Yoshida, Y., Joiner, J., Tucker, C., Berry, J., Lee, J.-E., Walker, G., et al. (2015). The 2010 Russian drought impact on satellite measurements of solar-induced chlorophyll fluorescence: Insights from modeling and comparisons with parameters derived from satellite reflectances. *Remote Sensing of Environment*, *166*, 163–177. https://doi.org/10.1016/j.rse.2015.06.008

Yu, L., Wen, J., Chang, C. Y., Frankenberg, C., & Sun, Y. (2019). High-resolution global contiguous SIF of OCO-2. *Geophysical Research Letters*, *46*(3), 1449–1458. https://doi.org/10.1029/2018gl081109

Zeng, Y., Badgley, G., Dechant, B., Ryu, Y., Chen, M., & Berry, J. A. (2019). A practical approach for estimating the escape ratio of near-infrared solar-induced chlorophyll fluorescence. *Remote Sensing of Environment*, *232*, 111209. https://doi.org/10.1016/j.rse.2019.05.028